COBEM 2023 27TH INTERNATIONAL CONGRESS OF MECHANICAL ENGENEERING

ABCM Brazilian Society of Mechanical Sciences and Engineering
27th ABCM International Congress of Mechanical Engineering
December 04-08, 2023, Florianópolis-SC, Brazil

COB-2023-2132
STUDY OF ENHANCED OIL RECOVERY BY LOW SALINITY WATERFLOODING IN DUAL-POROSITY MICROMODELS

Victor Bastos Braga Coelho
Fabiano Gilberto Wolf
UFSC, Microfluidics Laboratory (LabMicro), Rua Dona Francisca, 8300, Joinville, 89.219- 600, Brazil
victor.braga@posgrad.ufsc.br
fabiano.wolf@ufsc.br

Abstract. *Understanding the characteristics of fluid flow in porous media is necessary for optimizing oil recovery in reservoirs. As a result, microfluidics has proven to be an attractive method for the study of processes involving displacement oil at pore scale. The aim of the present study was to evaluate the impact of the geometry of porous media on enhanced oil recovery (EOR) processes. Two micromodels manufactured in polydimethylsiloxane (PDMS) were used. The M1 micromodel contains a pore network composed only of connected macrochannels and solid grains, while the M2 micromodel contains a double porosity network, with macrochannels and micropore grains. Initially, the microdevices were filled with high salinity brine (HS). Afterwards, fluorinated oil (FC-3283) was injected until maximum oil saturation was obtained, followed by the injection of HS to observe the water-oil displacement. Finally, low salinity brine (LS) was injected into the system as enhanced oil recovery (EOR). The recovery process was evaluated based on the analysis of high resolution images. The low salinity waterflooding (LSWF) proved capable of recovering an additional amount of valuable oil, presenting greater efficiency in the model with low permeability (M1). Such results indicate a relationship between rock morphology, absolute permeability and low salinity waterflooding efficiency.*

Keywords: *Microfluidics, Enhanced Oil Recovery (EOR), Dual-Porosity, Two-Phase Flow, Low Salinity Waterflooding.*

1. INTRODUCTION

The recovery rate of an oil reservoir is around 20 to 40%. The depletion of known reservoirs and the growing demand for hydrocarbons becoming this number unsustainable and leading to the need to develop solutions to optimize the extraction of this resource (Lifton, 2016). Thus, to optimize oil recovery, it is necessary to understand the physics behind the flow of fluids in porous media, which has been possible thanks to advances in the field of microfluidics, which, using micromodels of porous systems, has enabled the study and a better understanding of the processes that involve the displacement and accumulation of oil in the pore scale.

Defined as the science that processes and manipulates small volumes of fluids (Whiteside, 2006), microfluidics has been proving to be a powerful and economically advantageous area of research for studies of reservoirs. Water-oil flow processes in porous media have a high degree of complexity and involve physical behavior on micrometric scales that include properties such as wettability and interfacial tension between fluids, which normally do not affect a flow on macroscopic scales and influence the dynamics transport and trapping of fluids in a reservoir (Gogoi and Gogoi, 2019; Saadat et al., 2021).

The application of microfluidics in the oil and gas industry began in the early 1950, when Chatenever and Calhoun (1952) performed experiments with glass spheres between two transparent plates to observe flow on a micro scale, and since then it has been widely used as a simple yet powerful experimental method to understand: the mechanisms of multiphase flow, the influence of wettability and pore space geometry, the use of enhanced oil recovery (EOR), injection of water and fluid exotics, CO_2 capture, hydraulic fracturing, geochemical interactions between fluids and carbonate rocks, among others, always aiming to optimize oil recovery rates (Fu, 2016; Lifton, 2016; Wang et al., 2017; Yu et al., 2019; Gaol et al., 2020; Saadat et al., 2021).

Produced from transparent materials, micromodels can be manufactured using a variety of techniques and materials, including simple and complex geometries, and can simulate sandstone or carbonate reservoirs, adapting very well to the objectives of the study to be developed (Karadimitriou and Hassanizadeh, 2012; Anbari et al ., 2018). Called a “laboratory on a chip” (Gunda et al., 2011), its main advantages are related to the reduced size of its experiments, bringing a reduction in fluid, energy and time consumption, in addition to providing good repeatability and direct observation fluid-fluid interaction and fluid-solid interaction (Liu et al., 2022).

The structure of the porous medium, as well as the natural wettability of the rocks, have a significant influence on the processes of displacement and trapping of oil in reservoirs. Studies such as those by Buchgraber et al. (2012), Yun et al. (2017) and Wolf et al. (2022) used heterogeneous micromodels, composed of macroscopic pores from a few

millimeters in diameter to microscopic pores of the order of micrometers, to understand the influence of microporosity on two-phase oil-water transport. Avendanõ et al. (2019), Karadimitriou et al. (2019) and Saadat et al. (2021) investigated the effect of rock wettability on the recovery factor through microfluidics. However, the quantification of the effect of these properties is still unclear, stimulating the development of a large volume of studies in academia.

The distribution and microporosity fraction of the reservoirs are dominant factors in the residual fluid saturation rate (Wolf et al., 2022). In addition, reservoirs with heterogeneous porous structures are typical of carbonate reservoirs (Cantrell and Hagerty, 1999) and have great prominence because they are the typical reservoirs found in the pre-salt layer in Brazil.

The fluid-fluid and solid-fluid interfacial forces control wettability, with ionic strength being the predominant factor controlling electrostatic forces. Thus, a change in ionic strength can potentially lead to a change in wettability, which can be achieved by injecting low salinity waterflooding (LSWF), reducing the ionic content of connate water and reinjecting it into the reservoirs. However, the LSWF process is highly complex, as inconsistencies have been reported in the literature related to the conditions needed to observe a positive effect of low salinity on recovery (Karadimitriou et al., 2019; Liu et al., 2022).

Hao et al. (2019), Katende and Sagala (2019), discussed the main mechanisms that result in improved oil recovery by low salinity waterflooding (LSWF) in carbonate reservoirs. Farhadi et al. (2022) investigated the impact of rock morphology on enhanced oil recovery and Manoorkar et al. (2021) studied the impact of heterogeneities on residual oil entrapment also in carbonates. Recent and comprehensive reviews focused on two-phase flow studies can be found in the literature, however, the use of micromodels to discuss the impact of pore heterogeneity on the results of low salinity water injection presents a new approach and represents an advance in microfluidics.

The objective of the present study was to analyze the impact of porous heterogeneity on oil recovery processes, highlighting the role of microporosity and low salinity waterflooding.

2. MATERIALS AND METHODS

2.1 Experimental setup

The experimental setup, figure 1, consisted of a Harvard Apparatus 11 Pico Plus Elite syringe pump (precision ±0.35%), a Hamilton glass syringe of 5000 µl or 1000 µl, coupled to a Tygon tube with an internal diameter of 500 µm. Pressure values were monitored by an Elveflow inlet pressure sensor (model MPS 70 mbar, accuracy up to ±0.5% of maximum range). High resolution images were captured from the Olympus Model SZX10 Stereo Microscope with a DP26 5.0 MP digital camera with a 0.5x objective lens and 2.0x focus magnification.

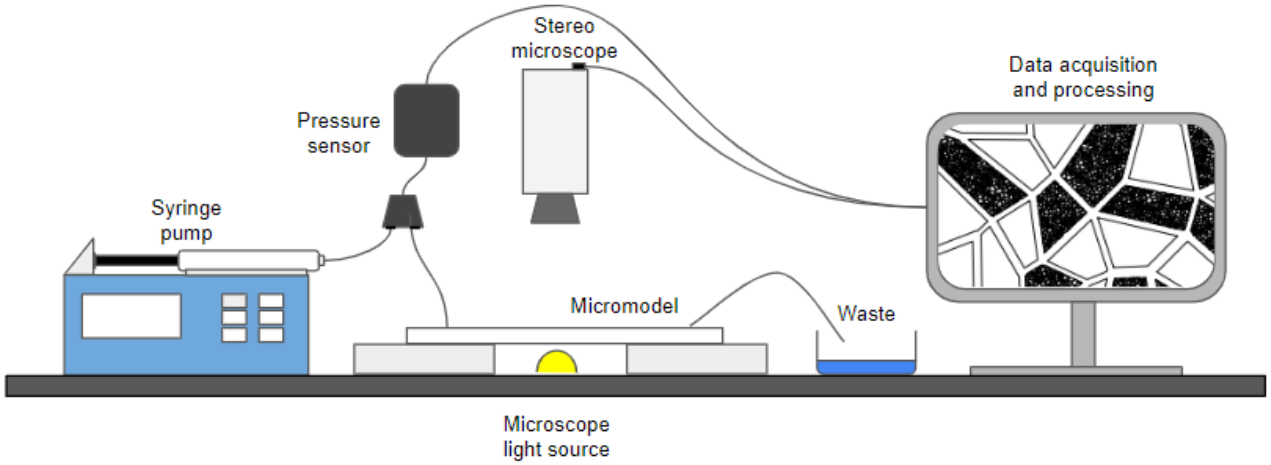

Figure 1: Schematic representation of the experimental setup. Dimensions shown are not to scale

2.2 Microfluidic device

Two types of micromodels manufactured in polydimethylsiloxane (PDMS) by the company FlowJEM using the soft lithography technique were used. The microchips were designed taking into account a bimodal distribution of pores, based on Voronoi tessellation, allowing the creation of a macroporous system composed of macroscopic channels and pores with different types of microporosity. The development of microdevice projects was presented in Wolf et al. (2022), resulting in the digital models as shown in figure 2. The device has dimensions of 6.8×3.0 cm^2 and channel depths of 31(0.5) µm and 34.8(0.9) µm, respectively for M1 and M2.

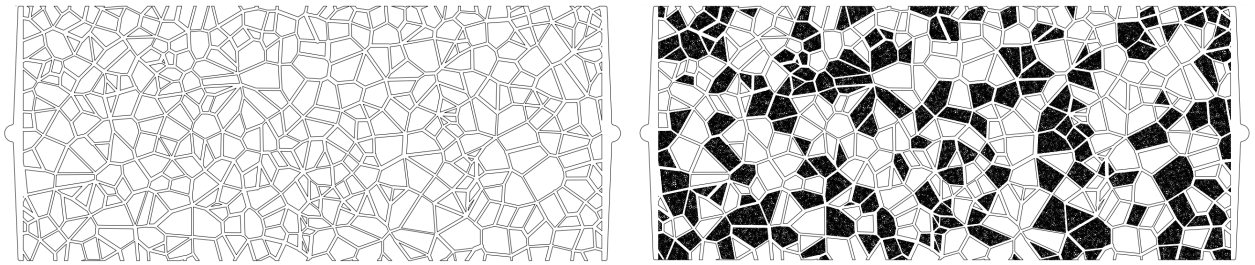

Figure 2: On the left, the M1 micromodel. On the right, the M2 micromodel, with macrochannels and some M1 solid grains converted into microporous grains (black).

The micromodel M1 contains a pore network composed only of macrochannels, ranging from 200 to 500 μm, and solid grains. The micromodel M2 contains a double porosity network, with macrochannels and grains with micropores, ranging from 20 to 50 μm, obtained from the transformation of originally solid grains in the M1 into microporous grains. The dual-scale geometry aims to include in the pore system one of the types of microporosity found in carbonates (Cantrell and Hagerty, 1999).

2.3 Fluids

Two brine solutions were prepared using deionized water with Talens Ecoline 578 dye and NaCl (Karadimitriou et al., 2019). High salinity (HS) brines, ionic strength of 0.6 M and viscosity, μ_{HS} = 1.14 mPa·s, were used representing sea water. Low salinity (LS) brines, ionic strength of 0.02 M and viscosity, μ_{LS} = 1.06 mPa·s, were used as the EOR method (Saadat, 2020). As a phase analogous to petroleum, fluorinated oil (FC-3283 from the company 3M) with viscosity μ_o = 1.3 mPa·s was used (Boukellal et al., 2009).

2.4 Experimental procedure

Naturally, the reservoir pores are saturated with formation brine before oil intrusion into the rocks occurs. Seeking to simulate the processes of saturation and exploration of a reservoir, the following steps were followed:
(1) saturation of the chip with the HS brine (formation water);
(2) chip saturation with FC (oil invasion);
(3) HS brine injection (secondary recovery);
(4) LS brine injection (advanced recovery).

At all stages, experiments were carried out at a laboratory temperature of 25°C and dynamic pressures were constantly monitored. Each experiment was repeated three times, carried out separately on three new micromodels. The values reported are the average of the three measurements with the standard deviation as error.

2.4.1. Initial saturation and characterization of micromodels

For optimization and elimination of air bubbles, the system was initially filled with CO_2 carbon dioxide (Wolf, 2022). Then, the HS brine was injected, maintaining the system pressure at around 100 mbar, adjusting the flow rate in the outlet tube through a valve, until the micromodels were completely saturated. Saturation is confirmed by visually inspecting the entire micromodel under the microscope.

Completely saturated, the micromodels were characterized in terms of porosity and permeability. Porosity calculations were performed by image analysis with ImageJ/Fiji open source software. For each micromodel, a high definition image was assembled from eighteen images of 2448 × 1920 pixels, using the TrakEM2 tool. After assembly, the images were binarized by color threshold based on saturation and brightness and then converted to 8-bit images. Saturation quantification was performed by counting the black pixels, which represent the areas occupied by colored water.

Absolute permeability measurements were performed based on Darcy's Law, where the relationship between the volume flow rate (Q) and the pressure drop ΔP through a porous medium is represented by

$$Q = \frac{kA\Delta P}{\mu L}, \tag{1}$$

where k, A, μ and L are, respectively, permeability, cross-sectional area, viscosity and model length. For both micromodels, a set of values of $\Delta P x Q$ was obtained following a cyclic process. The flow rate was increased in steps, up

to a maximum value, and then decreased in steps until reaching the initial value. Two cycles were performed for each experiment, totaling four pressure measurements for each imposed flow.

2.4.2. Oil invasion

Afterwards, FC-3283 was injected until maximum oil saturation was obtained. Started at a rate of 0.25 ml/h, the flow rate was slowly increased until reaching the system limit pressure, around 100 mbar. Final flow rates were 1 ml/h and 2.5 ml/h for M1 and M2, respectively. In total, 10 porous volumes were injected at the end of the process. Once the saturation was complete, the initial oil saturation (S_i) was calculated from the analysis of the images.

2.4.3. HS brine injection

Then, the HS brine was injected at a constant flow rate of 0.5 ml/h. After the breakthrough , the injection continued until at least 10 porous volumes were injected and no changes in the fluid distributions were observed. From the analysis of the images, the final oil saturation (S_f) was calculated.

The recovery factor (RF) is then calculated as the ratio of the extracted oil to the original oil on site, given by

$$RF = \frac{S_i - S_f}{S_i}. \quad (2)$$

2.4.4. LS brine injection

After the HS brine injection, LS brine was introduced into the net as a tertiary recovery stage. LS was injected at a flow rate of 0.5 ml/h. After the breakthrough, the injection continued until at least 10 porous volumes were injected and no changes in the fluid distributions were observed. Finally, the final oil saturations and recovery factors were calculated for both models following the previous item.

3. RESULTS AND DISCUSSION

3.1 Porosity and absolute permeability measurements

Table 1 presents the results of the porosity and permeability measurements of the micromodels. The absolute permeability was extracted from the linear relationship between the monitored values of flow and pressure. As seen in Figure 3, the relationship $Qx\Delta P$ for models M1 (blue curve) and M2 (red curve) had an excellent linear fit, respecting the behavior expected by Darcy's Law.

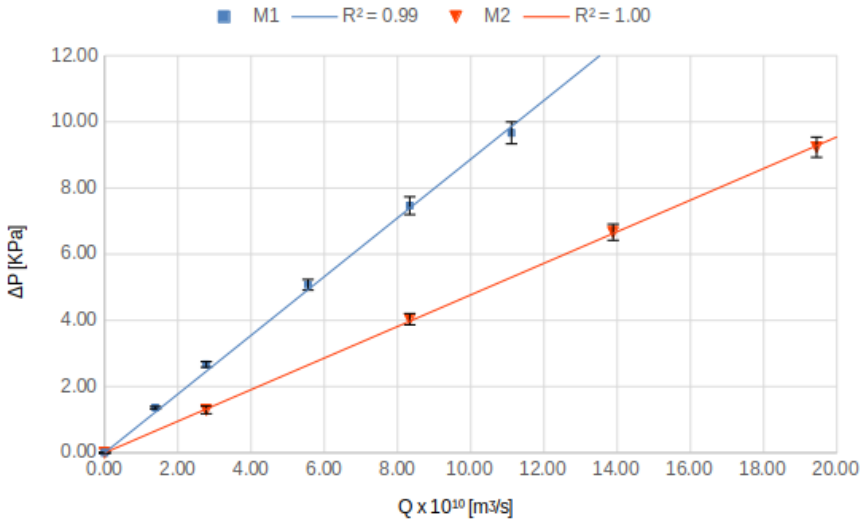

Figure 3: Relationship between pressure drop and volumetric flow rate for the micromodel M1 (blue) and M2 (red) with respective linear adjustment curves. The error bars were plotted considering the standard deviation in the measurements.

Table 1 - Porosity and permeability of micromodels M1 and M2 with standard deviation of three measurements.

MODEL	POROSITY [%]	PERMEABILITY [D]
M1	27.62 ± 0.16	10.11 ± 0.36
M2	41.74 ± 0.61	18.16 ± 1.10

With an increase of about 51% in porosity, due to the conversion of grains into microporous structures, the micromodel M2 had a considerable increase in permeability compared to the pure macroporous model M1. This is due to the fact that with this conversion, new channels were created, adding pathways for fluid flow. In addition, it is important to highlight that the permeability increased by 79%, a value above the increase in porosity, evidencing the direct, but not proportional, relationship of ϕ and K.

3.2 High Salinity Water Injection

Figures 4 and 5 show the comparisons between initial (S_i) and final (S_f) saturations for models M1 and M2, respectively. A similar pattern is observed in filling and oil displacement in the macrochannels in both models, highlighting the efficient oil displacement in the horizontal channels, parallel to the oil-HS displacement.

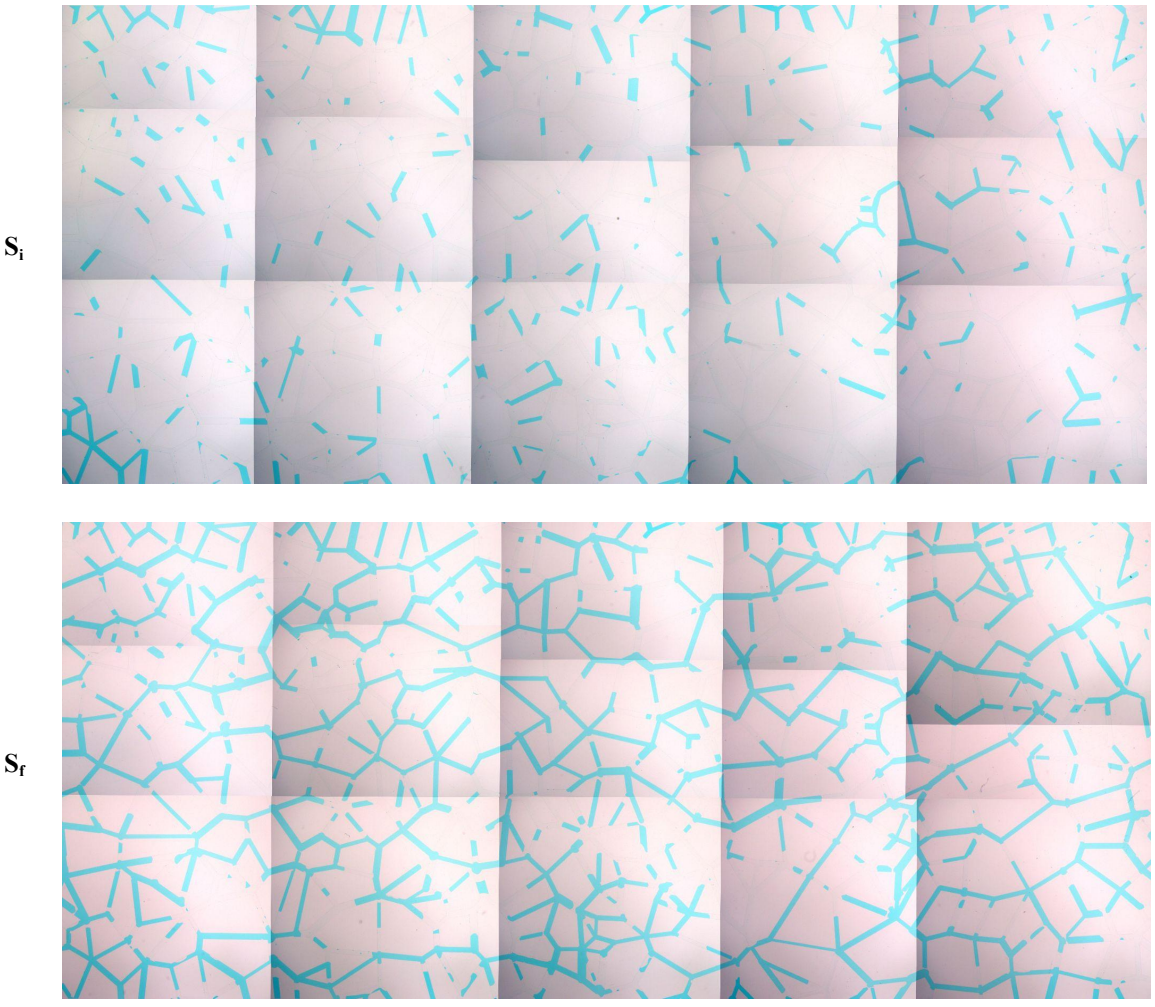

Figure 4: M1 initial (S_i) and final (S_f) distribution of HS-oil after breakthrough. The blue color represents the HS brine.

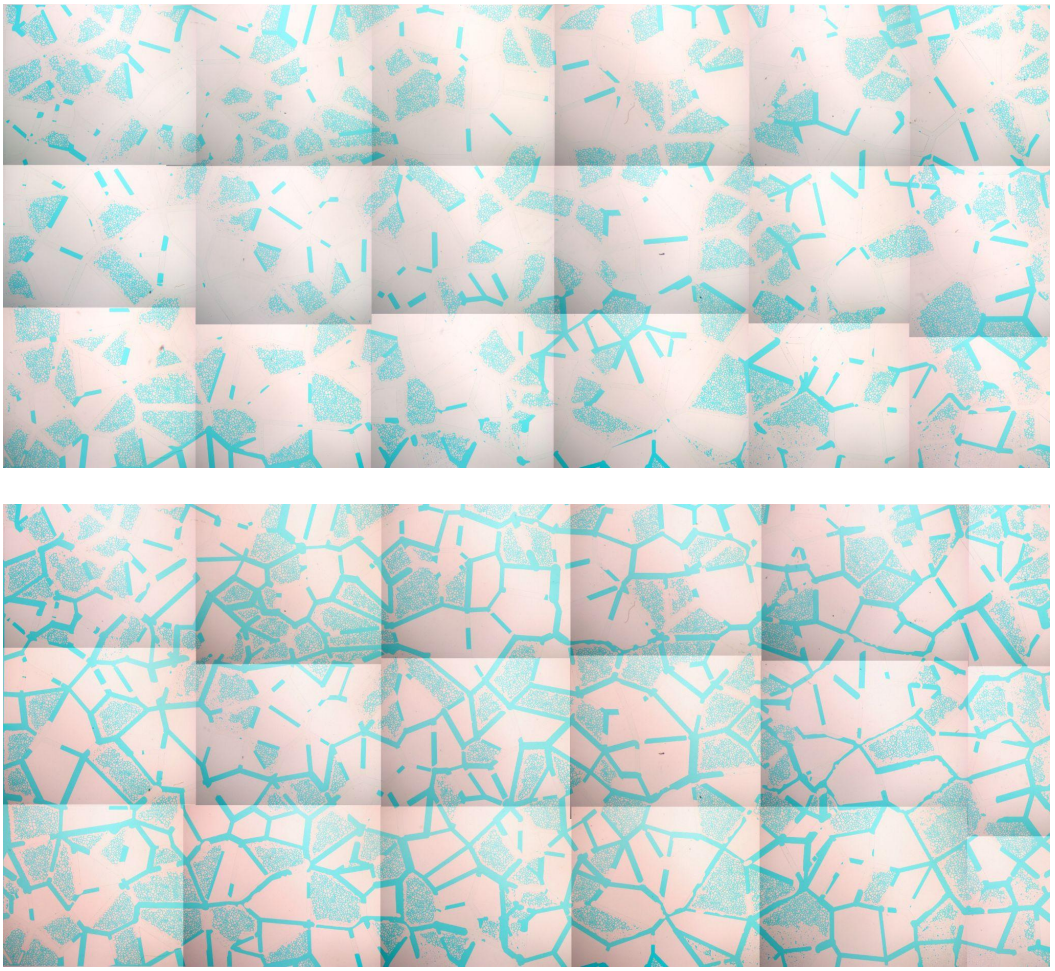

Figure 5: M2 initial (S_i) and final (S_f) distribution of HS-oil after breakthrough. The blue color represents the HS brine.

Figure 6 shows a highlighted microporous region of the M2 model, showing that the oil migration process, step 2, was unable to access the central regions of the microporous grains, occupying only the external part of the microporous grains. Although the injection of HS showed great efficiency in displacing the oil in the macrochannels, the microchannels were not effectively affected, meaning that a large part of the oil trapped in the microporous regions was not mobilized. In addition, observing the oil-water interface, it is possible to visualize that the displacement of the oil by the HS occurred through a drainage process, displaced fluid wets the reservoir, which brought additional difficulty to the movement of oil in the microchannels. Although not evidenced by the visual analysis of Figures 4 and 5, table 2 shows a higher RF for the M2 model.

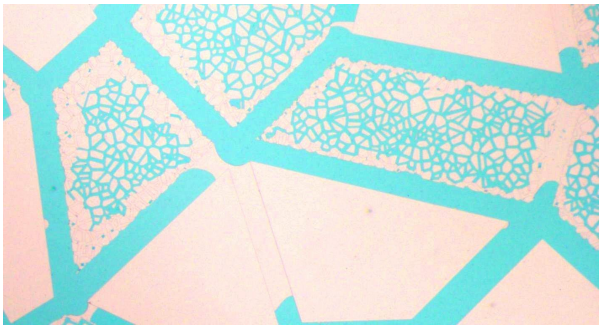

Figure 6: Highlight of microporous region after breakthrough. The blue color represents the HS brine.

Table 2 presents the results after analyzing the images for the initial (S_i) and final (S_f) saturations and the recovery factor (RF) of the two models. The results show that the conversion of solid grains into microchannels, in the M2 model, created new flow paths, increasing connectivity and assisting in the mobilization and displacement of oil. This increase in connectivity favored flow, which meant that HS moved the oil more efficiently, with emphasis on the mobilization of fluids present in the macrochannels.

Table 2: Comparison of results for initial (S_i), final (S_f) saturations and recovery factor (RF) with standard deviation of three measurements.

MODEL	S_i	S_f	RF
M1	0.75 ± 0.02	0.35 ± 0.01	0.53 ± 0.01
M2	0.60 ± 0.04	0.27 ± 0.01	0.55 ± 0.02

3.3 Low Salinity Waterflooding (LSWF)

Figures 7 and 8 show the comparison between the final HS and LS saturations for the M1 and M2 models, respectively, and the RF can be seen in Table 3.

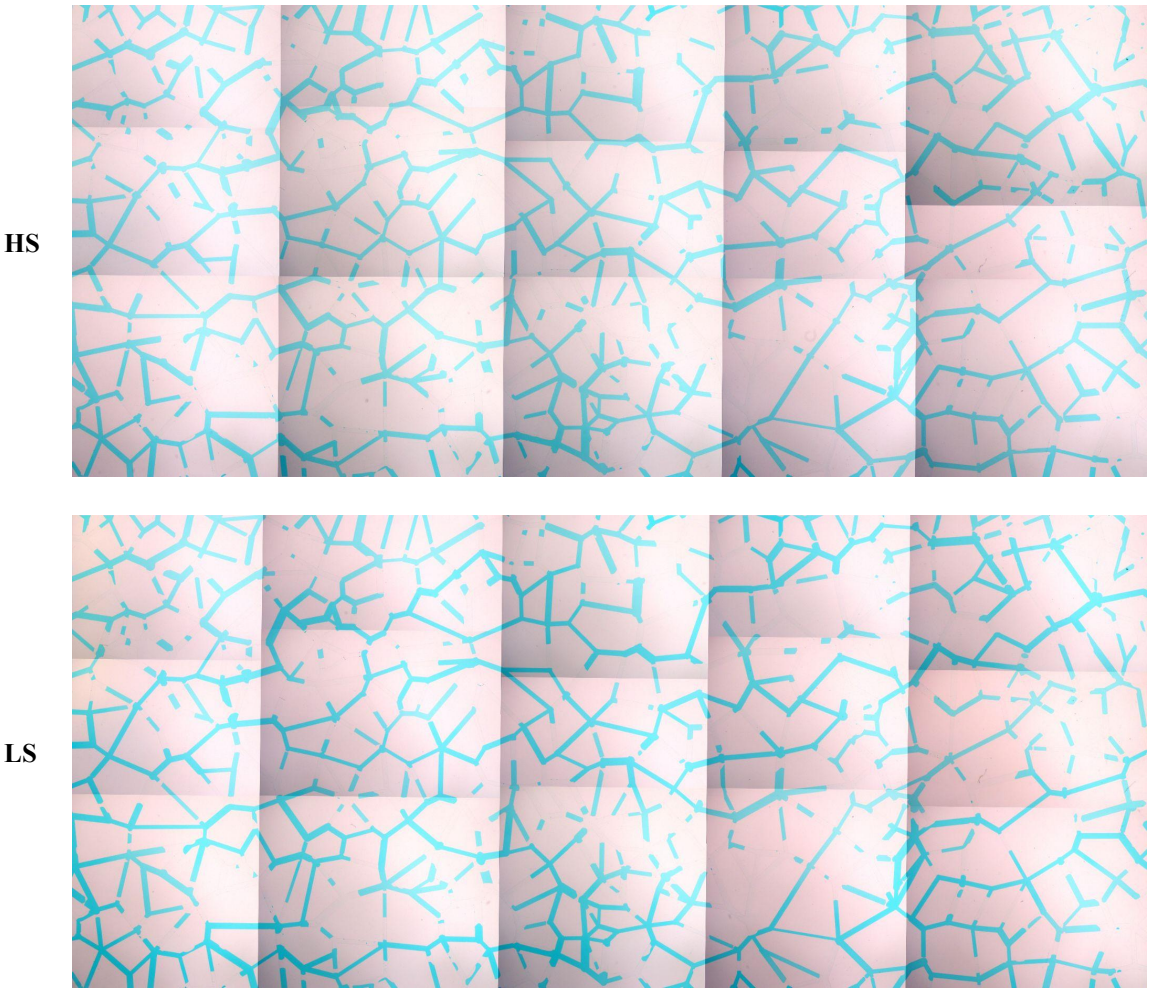

Figure 7: M1 final oil saturations for HS and LS injection after breakthrough.

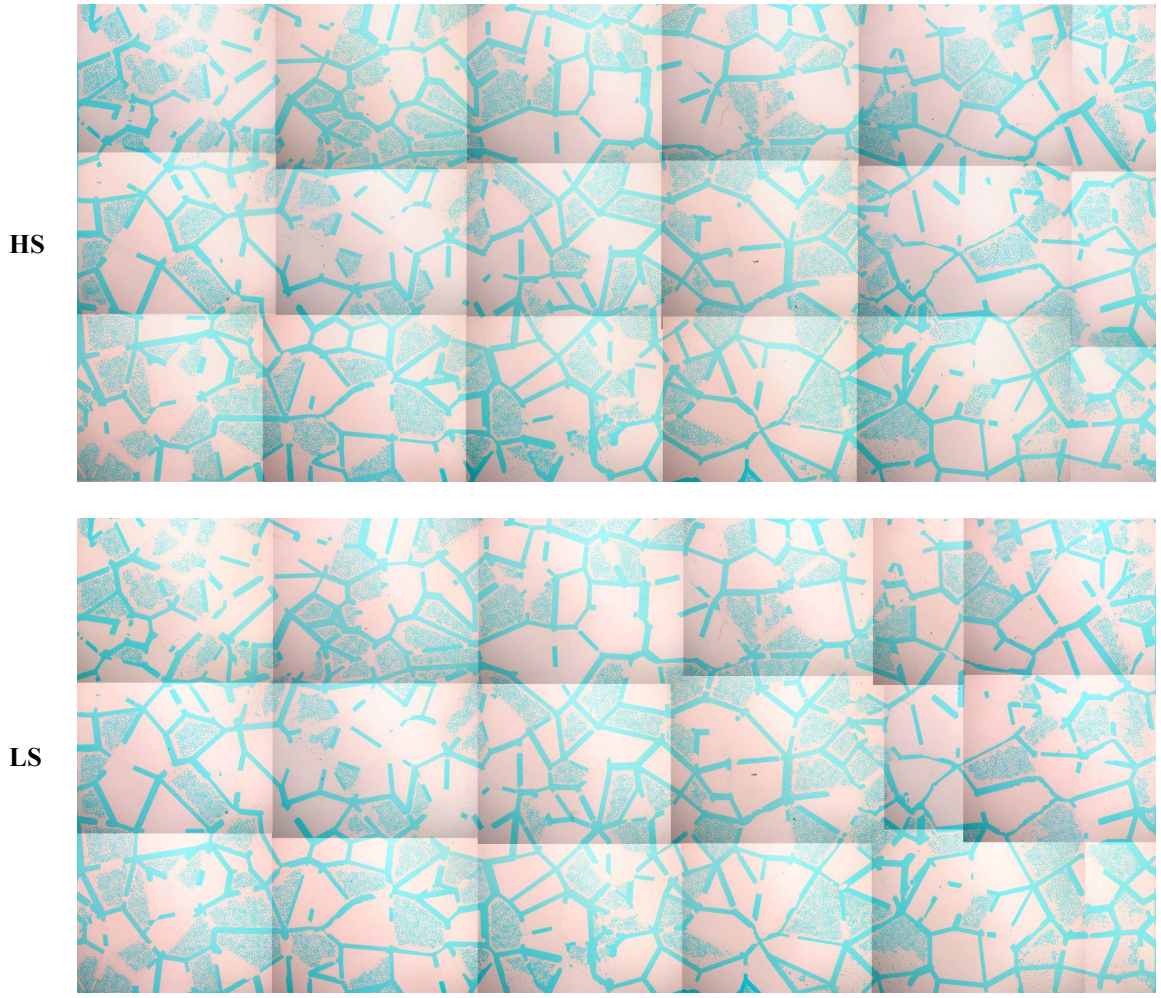

Figure 8: M2 final oil saturations for HS and LS injection after breakthrough.

Figure 9 presents the comparison between the secondary and tertiary recovery factors (RF) for the two micromodels. In all models, LS injection as tertiary recovery generated additional oil recovery. In the end, models M1 and M2 presented the same recovery factor, however, M1 obtained a greater increase compared to M2.

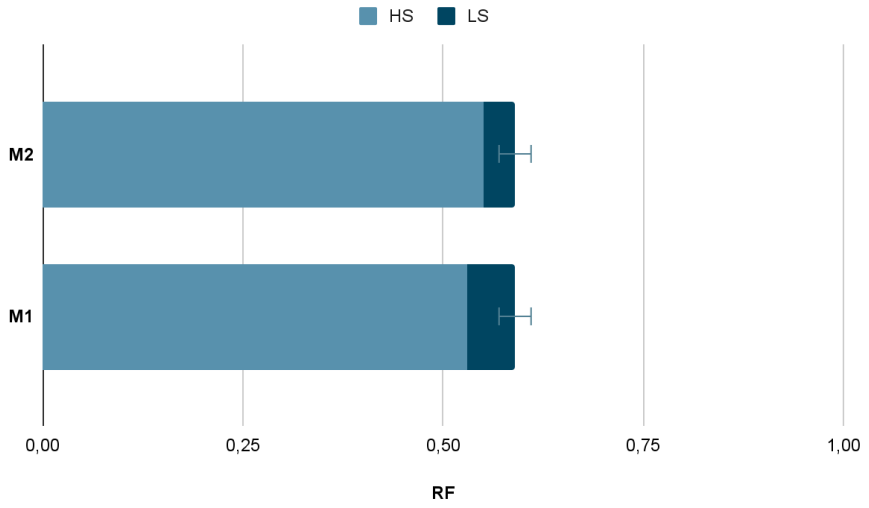

Figure 9: Comparison between secondary (HS) and tertiary (LS) recovery factors (RF), with the standard deviation of measurements.

Table 3: Comparison between the RFs of the HS and LS injection in the M1 and M2 micromodels with standard deviation of three measurements.

MODEL	RF HS	RF LS
M1	0.53 ± 0.01	0.59 ± 0.02
M2	0.55 ± 0.02	0.59 ± 0.02

Different studies have reported a wide range of RFs from 0.00 to 19.53% for LS injection after HS injection, depending on the type of reservoir and fluids used (Saadat et al, 2020; Chávez-Miyaucht et al, 2020 and Saadat et al. 2021), which shows the relationship between the results and the existing literature.

The increase in RFs was 10.0% and 7.1% respectively for M1 and M2. This result emphasizes the role of porous geometry in the performance of LS injection as tertiary recovery and showed that the model with higher permeability (M2) presented lower additional oil recovery compared to the model with low permeability (M1). Although research into the possible effect of pore geometry on the effectiveness of LS injection is still very limited, investigations into the impacts of porous heterogeneity in carbonates indicate a relationship between rock morphology, absolute permeability and LSWF efficiency.The literature attributes the additional oil recovery in low permeability geometries to the large rock surface exposed to brine compared to high permeability geometries, evidencing a relationship between permeability and LSFW efficiency (Li et al., 2020 and Farhadi et al., 2022).

4. CONCLUSION

The objective of the present study was to evaluate the impact of the characteristics of porous media on EOR processes. The conversion of porous grains into microchannels, in the M2 model, created new flow paths, helping to mobilize and displace oil in the macrochannels, which favored the drainage process in these regions. It was possible to observe a similar pattern in the filling and displacement of oil in the macrochannels of both models, highlighting the efficient displacement of oil in the horizontal channels. The LS injection proved capable of recovering an additional amount of valuable oil, presenting greater efficiency in the model with low permeability (M1). The results are in line with current literature and demonstrate a relationship between porous geometry and the efficiency of LSFW as an EOR method.

5. ACKNOWLEDGMENTS

The authors would like to thank Petrobras for its financial support.

6. REFERENCES

Anbari, A., Chien, H., Datta, S. S., Deng, W., Weitz, D. A., Fan, J., 2018, Microfluidic model porous media: Fabrication and applications, Small , vol 14(18).

Avendaño J., Lima, N., Quevedo, A., Carvalho, M., 2019, Effect of surface wettability on immiscible displacement in a microfluidic porous media. Energies, vol. 12(4), pp .664.

Boukellal, H., Selimovic, S. Jia, Y., Cristobal, G., Fraden, S., 2009, Simple, robust storage of drops and fluids in a microfluidic device, Lab on a chip, vol. 9, pp. 331.

Buchgraber, M, Al-Dossary, M, Ross, C. M., Kovscek, A. R., 2012, Creation of a dual-porosity micromodel for pore-level visualization of multiphase flow, Journal of Petroleum Science and Engineering, Vol. 86, pp. 27.

Chávez-Miyauch, T. E., Lu, Y. Firoozabadi, A, 2020, Low salinity water injection in Berea sandstone: Effect of wettability, interface elasticity, and acid and base functionalities, Fuel, vol. 263, pp. 116572.

Chatenever, A., Calhoun, J. C. J., 1952, Visual examinations of fluid behavior in porous media: Part 1. Petroleum Transactions, AIME, vol. 195, pp. 149.

Farhadi, H., Ayatollahi, S., Fatemi, M., 2022, Impact of rock morphology on the dominating enhanced oil recovery mechanisms by low salinity waterflooding in carbonate rocks, Fuel, 2022, volume 324, part C.

Fu, T., 2016, Microfluidics in CO2 capture, sequestration, and applications. Advances in microfluidics - New applications in biology, energy, and materials sciences, IntechOpen, vol. 23.

Gaol, C. L., Wegner, J., Ganzer, L., 2020, Real structure micromodels based on reservoir rocks for enhanced oil recovery (EOR) applications. Lab Chip, vol. 20, pp. 2197.

Gogoi, S., Gogoi, S. B., 2019, Review on microfluidic studies for EOR application, Journal of Petroleum Exploration and Production Technology, vol. 9, pp. 2263.

Gunda, N. S. K., Bera, B., Karadimitriou, N. K., Mitra, S. K., Hassanizadeh, S. M., 2011, Reservoir-on-a-chip (ROC): A new paradigm in reservoir engineering, Lab Chip, vol. 11, pp. 3785.

Hao, J., Mohammadkhani, S., Shahverdi, H., Esfahany, M.N., Shapiro, A, 2019, Mechanisms of smart waterflooding in carbonate oil reservoirs - a review., J. Petrol. Sci. Eng., vol. 179, pp. 276,

Karadimitriou, N. K., Hassanizadeh, S.M., 2012, A review of micromodels and their use in two-phase flow studies, Vadose Zone J., vol. 11(3), pp. 215.

Karadimitriou, N. K., Mahani, H., Steeb, H., Niasar, V., 2019, Nonmonotonic effects of salinity on wettability alteration and two-phase flow dynamics in PDMS micromodels, Water Resources Research, vol. 55, pp. 9826.

Katende, A., Sagala, F., ,2019, A critical review of low salinity water flooding: Mechanism, laboratory and field application, Journal of Molecular Liquids, vol 278, pp. 627.

Lifton, V. A., 2016, Microfluidics: an enabling screening technology for enhanced oil recovery (EOR), Lab Chip, vol. 16, pp. 1777.

Li, S., Jackson, M. D., Agenet, N., 2020, Role of the calcite-water interface in wettability alteration during low salinity waterflooding. Fuel, vol. 276, p. 118097.

Liu, J., Zhang, Y., Wei, M., He, X., Bai, B., 2022, Fabrications and applications of micro/nanofluidics in oil and gas recovery: A comprehensive review, Energy Fuels, vol. 36, pp. 9904.

Manoorkar, S., Jackson, S. J., & Krevor, S., 2021, Observations of the impacts of millimeter to centimeter scale heterogeneities on relative permeability and trapping in carbonate rocks, Water Resources Research, vol. 57.

Saadat, M., Tsai, P. A., Ho, T., Oye, G., 2020, Development of a microfluidic method to study enhanced oil recovery by low salinity water flooding, ACS Omega, vol. 5, pp. 17521.

Saadat, M., Yang, J., Dudek, M., Oye, G., Tsai, P. A., 2021, Microfluidic investigation of enhanced oil recovery: The effect of aqueous floods and network wettability, Journal of Petroleum Science and Engineering, vol. 203, pp. 108647.

Wang, W., Chang, S., Gizzatov, A., 2017, Toward Reservoir-on-a-chip: Fabricating reservoir micromodels by in situ growing calcium carbonate nanocrystals in microfluidic channels, ACS Appl. Mater, Interfaces, vol. 9, pp. 29380.

Whitesides, G. M., 2006, The origins and the future of microfluidics, Nature, vol. 442 (7101), pp. 368.

Wolf, F. G., Siebert, D. N., Carreño, M. N. P., Lopes, A., Zabot, A. M., Surmas, R., 2022, Dual-porosity micromodels for studying multiphase fluid flow in carbonate rocks, Lab on a Chip, vol. 22, pp. 4680.

Yu, F., Jiang, H, Xu, F.; Fan, Z., Su, H., Li, J., 2019, New insights into flow physics in the EOR process based on 2.5D reservoir micromodels. Journal of Petroleum Science and Engineering, vol. 181, pp. 106214.

Yun, W., Ross, C. M.; Roman, S., Kovscek, A. R., 2017, Creation of a dual-porosity and dual-depth micromodel for the study of multiphase flow in complex porous media, Lab on a Chip, vol. 17, pp. 1462.

7. RESPONSIBILITY NOTICE

The authors are the only responsible for the printed material included in this paper.